Photocatalytic, spectroscopic and transport properties of lanthanide-doped TiO_2 nanocrystals

2006 J. Phys.: Condens. Matter 18 S2149

(http://iopscience.iop.org/0953-8984/18/33/S30)

INSTITUTE OF PHYSICS PUBLISHING JOURNAL OF PHYSICS: CONDENSED MATTER

J. Phys.: Condens. Matter **18** (2006) S2149–S2160 doi:10.1088/0953-8984/18/33/S30

Photocatalytic, spectroscopic and transport properties of lanthanide-doped TiO_2 nanocrystals

M Bettinelli[1], A Speghini[1], D Falcomer[1], M Daldosso[1], V Dallacasa[2] and L Romanò[3]

[1] Scientific and Technological Department, University of Verona and INSTM, Udr Verona, Italy
[2] Laboratory for Materials Analysis, Scientific and Technological Department, University of Verona, Italy
[3] Physics Department, University of Parma, Italy

Received 31 January 2006
Published 4 August 2006
Online at stacks.iop.org/JPhysCM/18/S2149

Abstract

The photocatalytic properties of the anatase form of nanocrystalline TiO_2 doped with lanthanide ions (Eu^{3+}, Sm^{3+} and Er^{3+}), obtained by a sol–gel preparation method, are studied by means of the degradation of methylene blue. It is observed that the presence of Sm^{3+} ion as a dopant significantly improves the photocatalytic activity of anatase TiO_2 with respect to the Eu^{3+} or Er^{3+} ions.

For the understanding of such a catalytic process the charge transport in these systems is studied by an appropriate Monte Carlo simulation which includes phonons, charged impurities and traps. The obtained results evidence the important role of the traps for the transit of the electrons in the systems investigated here. They decrease the diffusion coefficient by about three orders of magnitude with respect to the bulk, from which it is possible to obtain a simple estimate of the reaction rate in agreement with experimental results. All the lanthanide-doped samples show a strong luminescence in the visible region. The emission bands are affected by a notable inhomogeneous broadening, indicating a high disorder of the crystalline environment of the lanthanide ions in the titania host.

1. Introduction

The application of mesoporous n-TiO_2 has received considerable attention since the discovery of its role in the photoelectrolysis of water [1] with hydrogen production and consequent energy production and in the photodegradation of organic substances in water and air [2, 3].

These phenomena occur under ultraviolet (UV) irradiation with a wavelength whose energy exceeds the band gap of TiO_2. To avoid the limitations of the ultraviolet and be able to use solar radiation, various attempts have been made to lower the band gap through doping processes with transition metals and reduction in hydrogen atmosphere [4–7]. An

appreciable shift of the absorbing power into the visible part of the spectrum has been reported by nitrogen [8] and carbon [9] doping, corresponding to a reduction of the gap to the value 2.32 eV with respect to 3.2 eV for the undoped material. Other oxides have been considered, like $InTaO_4$, as catalysts for hydrogen production through doping with Ni [10].

TiO_2 offers great potential as a material for use in the industrial technology of detoxifying wastewater [11]: since the process occurs under ambient conditions, the formation of photocyclized intermediate products, unlike in direct photolysis techniques, is avoided, the photocatalyst is inexpensive and has a high turnover.

The photocatalysis of polluted air streams [3] is often more efficient that the one of liquid waste streams. Gas phase kinetics allow reactions to occur much faster than in the liquid phase. This fact has led some people to utilize air stripping of pollutants from liquid phase for treatment in the gas phase. In the process of treating air streams, TiO_2 must be suspended on some sort of surface to allow the gas to pass over it and react. This is usually some sort of matrix with a high surface area, which the UV light is shone upon. In a photocatalytic experiment a solid phase is suspended in a solution or deposited on a substrate and it is illuminated by solar or ultraviolet radiation. Within the solid semiconductor, electrons are excited by photons to the conduction band. Charges of one sign are pushed to the surface and charges of opposite sign are pushed inwards by the electric field of the depletion layer. On the surface the charges react with adsorbed species within a liquid or gas phase leading to their reduction/oxidation.

The efficiency of TiO_2 as a photocatalyst is higher when it consists of a single phase in the anatase form [12]. In this paper we apply a sol–gel preparation method to obtain nanocrystalline TiO_2 in the anatase form doped with lanthanide ions and test its photocatalytic properties by analysing the degradation of a dye (methylene blue), normally used as a probe in these kinds of experiment [13]. Sol–gel synthesis is an easy and rapid method to obtain single phase anatase TiO_2 [14–16] which may also be successfully doped with metal or non-metal ions. We have applied a sol–gel preparation method to obtain nanocrystalline TiO_2 in the anatase form doped with lanthanide ions. The use of lanthanide ions as dopants in our context has a two-fold aim: to increase the catalyst performance [17] and to yield a material with spectroscopic properties exploitable in many technological applications such as optoelectronic devices and materials for illumination [18]. The luminescence properties of the obtained samples have been studied by using laser excited emission spectroscopy. On realizing that the transport of photoinduced carriers within TiO_2 is of primary importance for the understanding of the catalysis process, we implement and apply a Monte Carlo simulation to study the charge transport, including the diffusion coefficient and the energy distribution in the presence of phonons, charged impurities and traps. Our results indicate that a consistent number of traps are responsible for the transit of charges through the systems investigated here.

2. Experimental section

2.1. Sample preparation

The starting materials were titanium(IV) butoxide (Aldrich, 97%), $Eu(NO)_3{\cdot}5H_2O$ (Aldrich, 99.9%), $Er(NO)_3{\cdot}5H_2O$ (Aldrich, 99.9%), $Sm(NO)_3{\cdot}6H_2O$ (Aldrich, 99.9%), absolute ethanol, and HCl (37 %). 30.0 ml of ethanol, 0.8 ml of HCl, 6.0 ml of titanium(IV) butoxide and an appropriate quantity of dopant were stirred for 4 h. The solvent was evaporated at 333 K until the xerogel was formed. The obtained xerogel was heat treated at 773 K for 5 h. In all cases the nominal molar ratio between titanium and the lanthanide ion was 99:1. Hereafter the samples are labelled TiO_2:Sm, TiO_2:Eu and TiO_2:Er.

2.2. Photocatalysis experiments

Samples of 50 mg of catalyst were finely ground in an agate mortar and dispersed in water. The suspensions were sonicated for 15 min. Subsequently the dye was added in order to have a concentration of 10 mg l^{-1}. Methylene blue is an organic dye which has the absorption maximum at 664 nm [13]. After the complete adsorption of the dye on the catalyst (about 15 min [13]), the suspensions were exposed to solar light for a total time of 7 h. The photocatalytic activity of our samples was compared to that of the commonly used reference material Degussa P25.

The kinetics of the methylene blue degradation was followed by measuring the absorbance of the filtered solution with a conventional double-beam UV/vis spectrometer at a wavelength of 664 nm.

2.3. Raman and emission spectroscopy

The 488.0 nm line of a Spectra-Physics Stabilite 2017 argon laser was used to excite the luminescence and Raman spectra. The signal was dispersed with a 0.46 m monochromator with a 150 lines mm^{-1} grating and detected with an air cooled CCD device. All the spectroscopic measurements were performed at room temperature.

3. Results and discussion

3.1. Spectroscopy results

Preliminary x-ray diffraction and transmission electron microscopy (TEM) experiments indicate that the present samples consist of single phase anatase spherical nanoparticles, with no contamination of other titania phases [19]. Moreover, from the broadening of the diffraction peaks and the electron microscopy images, the average size of the nanoparticles is estimated to be about 10–12 nm. A detailed investigation of the structural and morphological properties of these materials lies outside the scope of the present paper and will be reported elsewhere.

Figure 1 shows the Raman spectrum of the nanocrystalline TiO_2:Sm sample, which appears to be representative also for those of TiO_2:Eu and TiO_2:Er. The characteristic Raman bands lying at 516 (a) and 640 cm^{-1} (b) (see figure 1) are ascribed to the anatase phase [20]. Moreover, the absence of any Raman band at 612 cm^{-1} confirms the complete absence of the rutile phase [21], in agreement with the x-ray results.

Figure 2 shows the kinetics of the photocatalytic degradation of methylene blue. The nanocrystalline TiO_2:Sm sample shows very good photocatalytic properties, comparable with Degussa P25. In this regard, it has been recently reported that thin films of TiO_2 doped with Sm^{3+} show high activity in the adsorption of molecules and could be used as gas sensors [22]. It is worth noting that the photocatalytic properties of TiO_2 anatase are determined by both the presence of dopant and the morphology of the sample. On the other hand, the morphology of the samples under investigation is most probably similar for all the samples, also considering that the concentration of the dopant ion in the titania host is low. Therefore, the presence of Sm^{3+} ion as a dopant significantly improves the photocatalytic activity of TiO_2 anatase with respect to the Eu^{3+}-doped or Er^{3+}-doped TiO_2 samples.

All the samples under investigation show a strong laser induced luminescence in the visible region. The luminescence spectra of TiO_2:Sm, TiO_2:Eu and TiO_2:Er samples are reported in figure 3, and they clearly testify the presence of the lanthanide ions in the TiO_2 host. The spectra consist of characteristic Eu^{3+}, Er^{3+} and Sm^{3+} emission bands due to 4f–4f transitions as assigned in figure 3. In agreement with previous literature results [17, 23], the luminescence

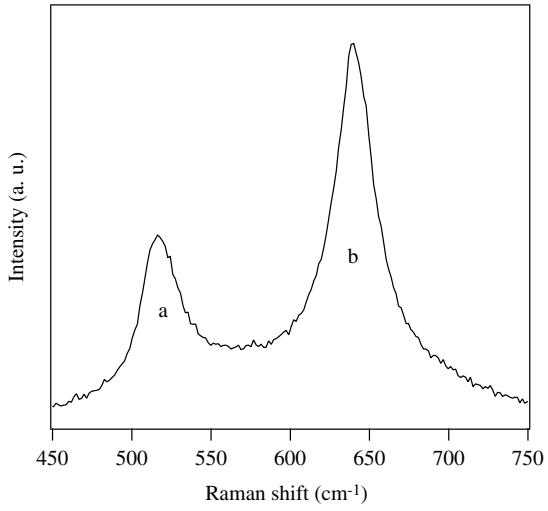

Figure 1. Room temperature Raman spectrum of the TiO_2:Sm sample.

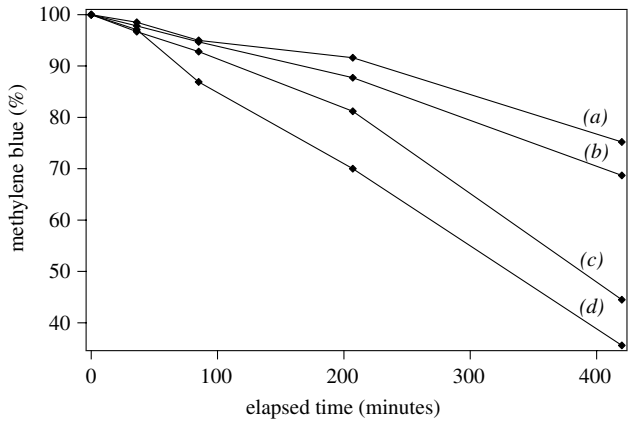

Figure 2. Kinetics of the photocatalytic degradation of methylene blue. The lines (*a*), (*b*), (*c*) and (*d*) correspond to TiO_2:Eu, TiO_2:Er, TiO_2:Sm, and Degussa P25 samples, respectively.

spectra of all samples are characterized by inhomogeneously broadened bands, typical of Eu^{3+}, Er^{3+} and Sm^{3+} doped disordered systems. As a measure of this behaviour, the FWHM of the $^5D_0 \rightarrow {}^7F_0$ emission band of the Eu^{3+} ion is 80 ± 2 cm^{-1}, confirming the high disorder of the crystalline environment of the Eu^{3+} ions in the TiO_2 host. In fact, the FWHM value is similar to those found for lanthanide-doped glass hosts [24]. The presence of such disorder is ascribed to the significant difference in the ionic radii in octahedral coordination for Ti^{4+} (74.5 pm) and Ln^{3+} (e.g. 108.7 pm for Eu^{3+}) [25], so the substitution of the dopant ion cannot easily occur without distortions, which could be affected by a site-to-site variation. Moreover, the necessary charge compensation could also occur in a variety of different ways, giving rise to a distribution of possible sites for Eu^{3+}. This broadening has been observed before for lanthanide ions doped in the anatase structure [26]. It is well known that the asymmetry ratio

$$R = \frac{I(^5D_0 \rightarrow {}^7F_2)}{I(^5D_0 \rightarrow {}^7F_1)}$$

of the integrated intensities of the $^5D_0 \rightarrow {}^7F_2$ and $^5D_0 \rightarrow {}^7F_1$ transitions can be considered indicative of the asymmetry of the coordination polyhedron of the Eu^{3+} ion [27]. In particular, the lower the R-value is, the higher is the site symmetry at the Eu^{3+} ion. The value of the

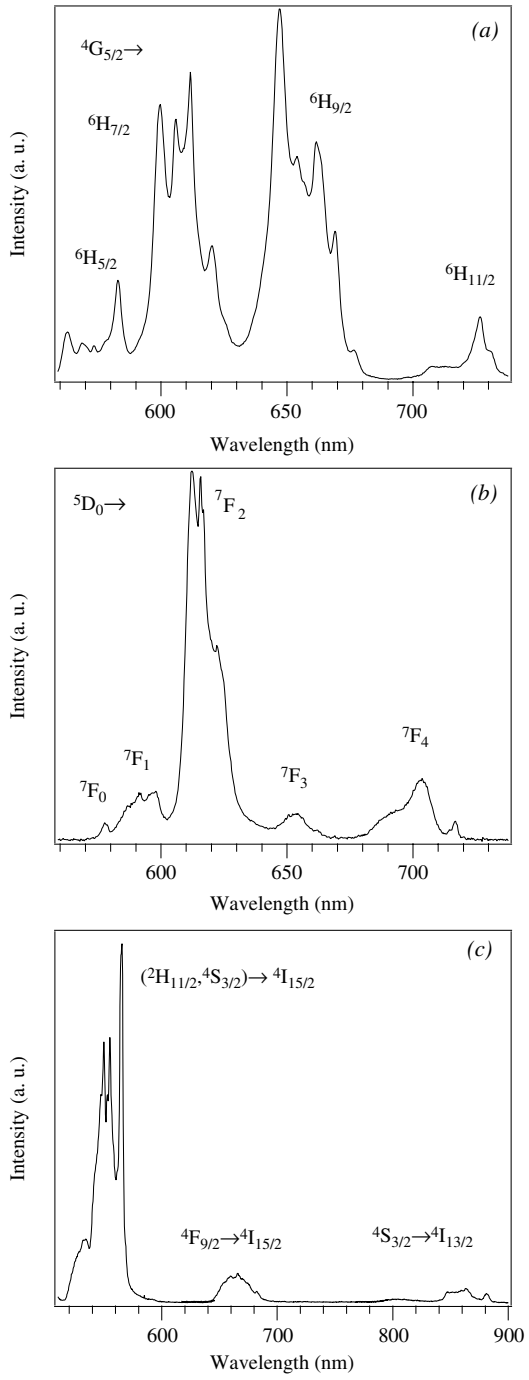

Figure 3. Room temperature luminescence spectra of the nanocrystalline TiO_2:Sm (*a*), TiO_2:Eu (*b*) and TiO_2:Er (*c*) samples ($\lambda_{exc} = 488.0$ nm).

asymmetry parameter for the TiO_2:Eu sample, obtained from the measured emission spectra (see figure 3(b)), results in being 7.5 ± 0.1. This value appears to be higher than those found for common Eu^{3+}-doped glass hosts, for which an *R*-value between 3 and 6 has been found [27]. It is interesting to note that the observed *R*-value is similar to that obtained for Eu-doped

zirconia films [27] and it is significantly higher than those found for bulk (5.3 ± 0.1) and nanocrystalline (6.5 ± 0.1) powders of the Eu^{3+}-doped cubic Y_2O_3 red phosphor [28]. This indicates that the coordination sphere of the Eu^{3+} ion for the present sample is on the average significantly more distorted than for bulk or nanocrystalline Eu^{3+}-doped yttria. Nevertheless, the R-value results in being lower than for Eu^{3+}-doped nanocrystalline TiO_2 powders prepared by a radio frequency thermal plasma oxidation technique ($R = 9.7$) [29]. Finally, the emission of the TiO_2:Eu sample is very efficient and comparable with that of the commercial phosphor YVO_4:Eu (QHK63 produced by Phosphor Technology, Hertfordshire, UK). In fact, from the luminescence spectrum of the commercial phosphor, measured in the same experimental conditions ($\lambda_{exc} = 488.0$ nm), we noted that the emission intensity of the TiO_2:Eu sample is only four times lower than the YVO_4:Eu one. Moreover, the strongest emission band of the TiO_2:Eu sample peaks at 610 nm, suggesting a possible use of the present material as a red phosphor for lighting devices.

3.2. Transport properties and Monte Carlo simulations

The understanding of catalysis in a nanosystem is dependent on the comprehension of transport of charge, in particular in the presence of traps. Since the surface to volume ratio is high, traps on the surface are expected to play a greater role than those in the bulk. Information on traps can be obtained, for example by experimental means including the time response of the electrons to an external time-varying input [30, 31], or by photocurrent/photovoltage spectroscopy [32, 33]. These studies indicate that transport occurs in the conduction band, but it is punctuated by trapping in deep states. From a theoretical point of view random Monte Carlo approaches have been suggested [34–36]. These studies have indicated the importance of trapping in the explanation of the electronic time-varying response. A Monte Carlo technique for a porous film has been introduced in [37] in which a random walk along chains of spherical grains is used while treating each grain as a bulk. In this model the electron transport phenomena occurring inside each grain are neglected and the whole transport is ascribed to traps on the surface of grains. Analytical procedures based on the solution of the continuity equation for both the free and trapped electron density have also been devised [38, 39], whose results turn out to compare well with the Monte Carlo ones. All of these approaches indicate that, as a result of traps, the modelling of the system can be achieved by an effective diffusion coefficient D_{eff} which depends on the electronic density and hence on the illumination [40, 41]. The low values of D_{eff} can be attributed to electronic motion in the band, interrupted by electronic trapping at states deep in the conduction band, typically 0.5 eV, and subsequent detrapping trough thermal excitation.

Experimental work on D_{eff} on the porous TiO_2 layer of Graetzel's cells [40–46] indicates that the value of D_{eff} is very much smaller than the value in the single crystal ($D \cong 10^{-2}$ cm^2 s^{-1}) [47] and falls in the range 10^{-4}–10^{-8} cm^2 s^{-1} [48–50], the higher value corresponding to higher illumination, typically $I \cong 10^{16}$ photons cm^{-2} s^{-1}.

The crystallographic structures of TiO_2 lead to phonon modes comprising contributions from acoustic and optical phonons along the directions of the cell which strongly couple with the conduction electrons. The strongest coupling occurs in rutile from LO optical modes, leading to polaronic effects. Values of the resistivity, thermopower, and Hall effect measurements on large single crystals of the anatase form of TiO_2 [51]and films [52] indicate an n-type mobility consistent with the scattering of carriers by the acoustic and optical phonons of TiO_2.

In the anatase crystal, oxygen vacancies are easily formed due to intrinsic oxygen deficiency. There is evidence, as a result, of the formation of shallow donor states [53] and the occurrence of very small activation energy ($\cong$0.004 eV) [51]. As regards nanocrystallites

in the anatase phase, phonon scattering is expected to be operating like in the single crystal since the electron mean free path $l = v_{\mathrm{th}} m D/kT \cong 8 \times 10^{-9}$ cm is smaller than the length of the system ($\cong$10 nm); impurity scattering from ionized centres is expected to originate from the doping of lanthanide ions and trapping centres are expected to cooperate, depending on the density of traps on the surface of the crystallites.

The Monte Carlo technique has been successfully used to study charge transport in semiconductors and insulator materials [54]. The method is based on a semiclassical description in which the motion of a sufficiently large number of electrons, subjected to scattering rates calculated by means of the usual perturbation theory, is followed for a given time t_{m}.

The electrons are injected at $t = 0$ into the crystal with an appropriate energy distribution $g(\varepsilon, 0)$ which is, generally, close to that expected at infinite time because we are interested in the study of the steady state of the system. Usually a constant electrical field is applied in the z-direction.

During the time t_{m} the state of motion of each electron is observed at regular time interval Δt to store the quantities z and x^2+y^2 related to the displacement of the electron in the field and transversal direction respectively. With a statistical average, one can obtain the drift velocity

$$w = \mathrm{d}\langle z\rangle/\mathrm{d}t \tag{1}$$

the transversal diffusion coefficient

$$D_{\mathrm{T}} = \frac{1}{4}\frac{\mathrm{d}}{\mathrm{d}t}\langle x^2 + y^2\rangle \tag{2}$$

and the lateral diffusion coefficient

$$D_{\mathrm{L}} = \frac{1}{2}\frac{\mathrm{d}}{\mathrm{d}t}\left\langle (z - \langle z\rangle)^2\right\rangle. \tag{3}$$

At low applied fields the drift velocity, as described by equation (1), presents a large statistical uncertainty originating from the thermal motion and, in this case, it is more convenient to obtain the ohmic mobility by means of the Einstein relation $\frac{kT}{e} = \frac{D_{\mathrm{T}}}{\mu}$ with D_{T} obtained by equation (2).

Further details on the Monte Carlo technique can be found in [54].

In this work we are interested in studying the transport properties of the two configurations of TiO_2 which are characterized by different effective mass and densities (rutile: $m^* = 20\ m_0$, $\rho = 4.2$ g cm^{-3}; anatase: $m^* = 9\ m_0$, $\rho = 3.2$ g cm^{-3}, m_0 being the bare electron mass). At zero external bias we simulate the motion of typically 10^5 electrons in an electrical field $E = 10^{-7}$ V m^{-1} (the non-zero value is used to avoid fluctuations of D and moderate increase of E up to 10^{-5} V m^{-1} does not significantly change the result for D) at temperature $T = 300$ K.

During the simulation the electrons suffer collisions with the lattice in which they can absorb and emit phonons and with the ionized impurities. After a flight, where the electron is accelerated by the electrical field, a scattering event is stochastically selected on the basis of its cross section. In our Monte Carlo simulation the scattering processes can be considered isotropic and the momentum transfer cross sections (weighted with the factor $(1 - \cos\theta)$) are used [55]. In order to evaluate the duration of electron flight between a two successive scatterings we use a Rees technique [56] in which the collision frequencies rather than the cross sections are needed.

To determine the collision frequencies of the electron–phonon interaction we use the golden rule of the perturbation theory and we obtain [57]

$$\left(\frac{1}{\tau}\right)_{\mathrm{el-ph}} = \frac{(2m^*)^{3/2} E_1^2 q \sqrt{\varepsilon \mp \hbar\omega}}{2\pi\rho\hbar^3 v_{\mathrm{s}}} \tag{4}$$

Table 1. Parameters used in the simulations.

Parameters	Values
E_1	3.16 eV
q	1×10^8 cm^{-3}
$\hbar\omega/2\pi$	0.016 eV
v_s	6.9×10^5 cm s^{-1}
N_i	10^{18} cm^{-3}
k	10
n_c	10^{20} cm^{-3}
ΔE	0.3 eV

where $\pm$ refers to the phonon absorption/emission, E_1 is the deformation potential, q the electron wavevector, ε the electron energy and v_s the sound velocity.

The expression (4) is obtained using a model with a constant frequency ω of an acoustic branch of the order of the Debye frequency, neglecting the wavevector dependence, as frequently done, in the self-energy expression for the electron–phonon interaction [58].

The scattering with the ionized impurities is described by a collision frequency [59]:

$$\left(\frac{1}{\tau}\right)_{\text{imp}} = \frac{\pi}{\sqrt{2m^*}} \frac{e^4 N_I}{k} \varepsilon^{-3/2} L(\varepsilon) \tag{5}$$

where N_I is the ionized impurity concentration and k the dielectric constant. In the expression (5) $L(\varepsilon) = \ln\left[2 + \left(\frac{k\varepsilon}{e^2 N_I^{1/3}}\right)^2\right]$.

The parameters used in our simulation are listed in table 1.

In figure 4 the temporal behaviour of the average quantity $\langle x^2 + y^2 \rangle$, as obtained by the simulation with the parameter of the table 1, is reported for the rutile and anatase systems. The perfect straight line indicates in both cases that the system reaches the steady state in a time less than 10^{-12}, which corresponds to about 100 scattering events for each electron. Just for a comparison, we report in figure 5 the temporal behaviour of $\langle z \rangle$ in the same time interval as in figure 4; as mentioned before, this quantity is affected by a large uncertainty at this very low electrical field. In the inset a comparison with the results obtained with a field $E = 10^4$ V cm^{-1} is reported. According to equation (2), from the slopes of the straight lines of figure 4, one extracts the transversal diffusion coefficients for rutile $D_T = 1.05 \times 10^{-2}$ cm^2 s^{-1} and for anatase $D_T = 1.42 \times 10^{-2}$ cm^2 s^{-1}. The good agreement of these values with those deduced from mobility data for single crystalline TiO_2 [47] confirms the choice of the scattering mechanisms and of the parameters to describe the transport properties of this material.

It should be noted that the presence of the ionized impurity is essential to obtain the previous results; in fact, during the time of simulation the 10^5 electrons suffer about 10^7 scattering events with the lattice while they collide with the impurities 10^{11} times. On the other hand, a simulation where only electron–phonon interactions are considered gives a value for D_T of the order of 10^{-1} cm^2 s^{-1}, which is an order of magnitude larger than the experimental value. From the simulation it is possible also to obtain the energy distribution as is shown in figure 6, where a comparison between two distribution functions $g(\varepsilon)$ are reported as obtained at two different fields in rutile. The Maxwellian shape of the function is in agreement with the classical theory and, as expected, at high field the electrons have a larger energy, as indicated by the energy tail.

In the second part of this work we introduce the possibility for the electrons to be trapped at an appropriate rate. In the first approximation we consider the effect of the trap concentration,

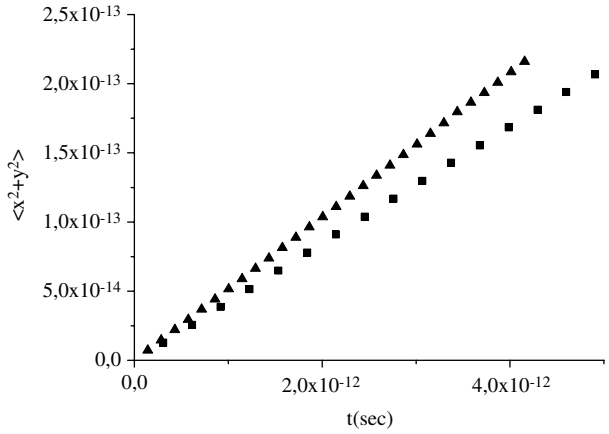

Figure 4. Temporal behaviour $\langle x^2 + y^2 \rangle$ obtained by the simulation with $E = 10^{-7}$ V m^{-1} for rutile (squares) and anatase (triangles). According to equation (2), from the slopes of the straight lines one obtains the transversal diffusion coefficients.

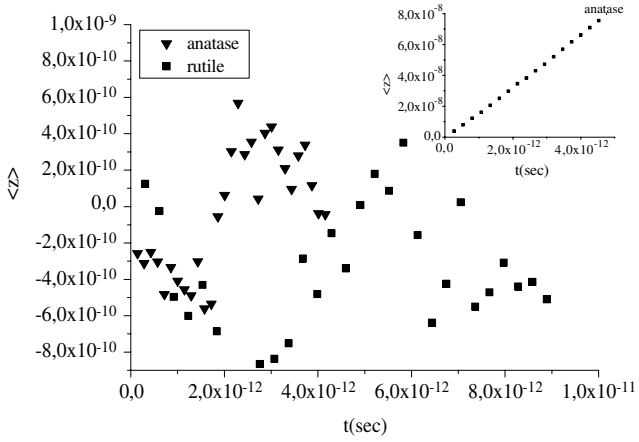

Figure 5. Temporal behaviour of $\langle z \rangle$ obtained by the simulation with $E = 10^{-7}$ V m^{-1}. Inset: the same quantity as in figure at $E = 10^4$ V m^{-1}.

on assuming that each atomic TiO_2 unit on the surface contributes one trap, and we obtain $n_{\text{trap}} \cong 10^{22}$ cm^{-3}. Then the trapping rate becomes

$$\left(\frac{1}{\tau}\right)_{\text{trap}} = n_{\text{trap}} v_{\text{th}} \sigma \tag{6}$$

where $\sigma \sim 10^{-16}$ cm^2 is the cross section per trap, and $v_{\text{th}} = \sqrt{3kT/m^*}$ is the thermal velocity [37].

A trapped electron can be detrapped at a rate [37]

$$\left(\frac{1}{\tau}\right)_{\text{det}} = \left(\frac{1}{\tau}\right)_{\text{trap}} n_{\text{c}} \exp\left(-\frac{\Delta E}{kT}\right) \tag{7}$$

where ΔE is the trap energy level referred to the conduction band and n_{c} is the electron concentration in the conduction band.

The parameters used in the simulation are reported in table 1.

In figure 7 we show the temporal behaviour of the quantity $\langle x^2 + y^2 \rangle$; in this case the presence of the trapping and detrapping events gives rise to the steady state in shorter times. From the slope of the straight line at larger time one can extrapolate the value of the transversal diffusion coefficient $D_{\text{T}} = 1.95 \times 10^{-5}$ cm^2 s^{-1}. This result appears surprisingly good if compared with the IMPS data [42] for which $D = 2 \times 10^{-5}$ cm^2 s^{-1} and it confirms that all

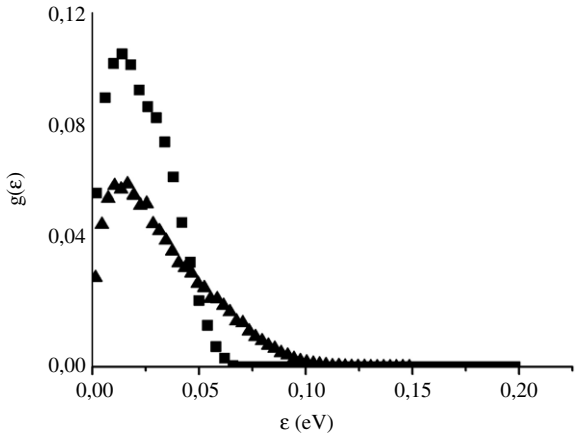

Figure 6. Comparison between the energy distribution obtained with $E = 10^{-7}$ V m^{-1} (squares) and $E = 10^{4}$ V m^{-1} (triangles).

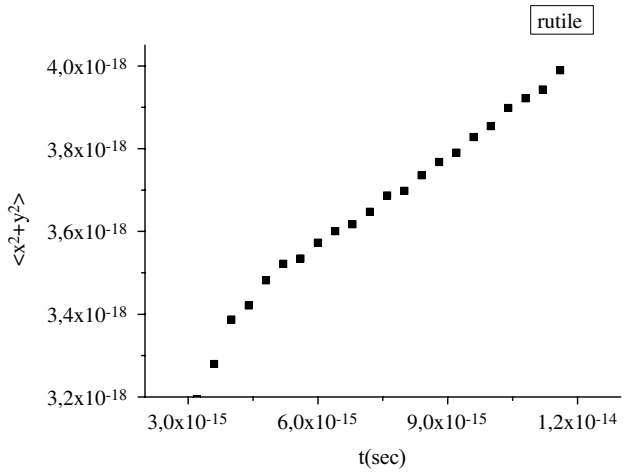

Figure 7. Temporal behaviour of $\langle x^2 + y^2 \rangle$ obtained with the simulation with trapping and detrapping events. According to equation (2), from the slope of the straight line one obtains the transversal diffusion coefficient.

the scattering mechanisms, including trapping, contribute to the transport properties of doped TiO_2. It should be noted also that in our case 122 electrons are trapped and only 10 of these are detrapped.

4. Conclusions

The parameters indicated in the previous paragraph indicate a small fraction of trapping/detrapping processes; in fact these are 10^{-3} (trapping) and 10^{-4} (detrapping) of the whole number of electrons considered in the simulation. Correspondingly, the value obtained for the diffusion coefficient may be viewed as an upper bound subject to a further depression with respect to the bulk value when the importance of the trapping is enhanced. This may happen if the cross section, which was put at 10^{-16} cm^2, is increased, i.e., when the dimension of the traps is increased. The reported values down to $D = 10^{-8}$ cm^2 s^{-1} may be a consequence of this. On the other hand, since the values of the diffusion coefficient for the single crystal are well reproduced by phonon and impurity scattering, it appears that the parameters assumed for the corresponding collision frequencies are to be considered as fixed to some extent, also in consideration of the fact that the density of impurities is low. In other words, it can be assumed that the trapping processes are mainly responsible for the lowering of the diffusion coefficient.

We can estimate an upper bound for the photocatalytic rate from the bound of the diffusion coefficient. We can assume that the rate at which an electron diffuses to the grain surface is $1/T$, where $T = r^2/D$ is the time to reach the surface, where r is the grain dimension. The reaction rate may then be evaluated as $R = (1/T)\,p\,n$, where p is the probability of finding the electron close to the dye and n the quantum efficiency for the photoextraction. p can be evaluated by the ratio between the number of dye molecules per grain N_{dyes} and the total number of TiO_2 units on the surface; this latter, on taking account of a typical unit cell dimension $a = 4 \times 10^{-8}$ cm, turns out to be about 8×10^3. The N_{dyes}-value can be estimated from the dye and TiO_2:Ln amounts used for the photocatalysis experiment, considering an average grain size of 10 nm for the titania nanoparticles [25]. In fact, the simple ratio between the number of dye molecules present in solution and the dispersed TiO_2 nanoparticles turns out to be in the range 15–20. A decrease of about 15% of the absorbance at 664 nm of the dye solution has been observed after the addition of the TiO_2 samples, at the beginning of the photocatalysis experiment (see section 2.2), indicating that only a fraction (about 1/7) of the total dye molecules is adsorbed at the titania surface. Therefore, we can estimate a value of $N_{\mathrm{dyes}} \approx 2$–3. For a grain size $r = 10$ nm we then have $p = 2.5 \times 10^{-4}$, and using $D = 10^{-5}$ cm^2 s^{-1}, as obtained by our Monte Carlo simulations, we have $R = 2.5 \times 10^{-3}$ s^{-1} for common values $n = 10^{-6}$. This estimated value appears in good agreement with the best rate indicated by the experimental results for the Sm-doped samples.

On the other hand, it should be noted that the time T, which turns out to be 10^{-7} s for the considered system, is very much longer than the extraction time, 10^{-13} s typically, due to the photoelectric effect, and it appears to be responsible for the time response of the photocatalytic process.

Acknowledgments

The authors gratefully thank Professor Stefano Enzo (University of Sassari, Italy) for the x-ray diffraction experiments, Professor Anna Musinu for the TEM experiments and Gerry Sorce (Phosphor Technology, Hertfordshire, UK) for providing us with the YVO_4:Eu (QHK63) sample. This work is part of a project co-financed by Fondazione Cariverona (Verona, Italy).

References

[1] Fujishima A and Honda K 1972 *Nature* **238** 37
[2] Hoffman M R *et al* 1995 *Chem. Rev.* **95** 69
[3] Matthews R W 1993 *Photocatalytic Purification and Treatment of Water and Air* ed D F Ollis and H Al-Ekabi (Amsterdam: Elsevier)
[4] Ghosh A K and Maruska G P J 1997 *Electrochem. Soc.* **24** 15
[5] Choi W *et al* 1994 *J. Phys. Chem.* **98** 13669
[6] Anpo M 1997 *Catal. Surv. Japan* **1** 169
[7] Akikusa J 1997 *Thesis* Duquesne University
[8] Asahi R *et al* 2001 *Science* **293** 269
[9] Shaked U *et al* 2002 *Science* **297** 2243
[10] Zou Z *et al* 2001 *Nature* **414** 625
[11] Kutal C and Serpone N 1993 *Photosensitive Metal Organic Systems: Mechanistic Principles and Applications* (Washington, DC: American Chemical Society)
[12] Diebold U 2003 *Surf. Sci. Rep.* **48** 53
[13] Lachheb H, Puzenat E, Houas A, Ksibi M, Elaloui E, Guillard C and Herrmann J-M 2002 *Appl. Catal.* B **39** 75
[14] Frindell K L, Bartl M H, Popitsch A and Stucky G D 2002 *Angew. Chem. Int. Edn* **41** 960
[15] Francisco M S P and Mastelaro V R 2002 *Chem. Mater.* **14** 2514
[16] Wilke K and Breuer H D 1999 *J. Photochem. Photobiol.* A **121** 49
[17] Hirano M and Date K 2005 *J. Am. Ceram. Soc.* **88** 2604
[18] Liqiang J, Xiaojun S, Baifu X, Baiqi W, Weimin C and Honggang F 2004 *J. Solid State Chem.* **177** 3375

[19] Falcomer D, Daldosso M, Speghini A, Bettinelli M, Enzo S, Lasio B, Musinu A and Cannas C 2006 unpublished results
[20] Ohsaka T, Izumi F and Fujiki Y 1978 *J. Raman Spectrosc.* **7** 321
[21] Porto S P S, Fleury P A and Damen T D 1967 *Phys. Rev.* **154** 522
[22] Lange S, Kiisk V, Reedo V, Kirm M, Aarik J and Sildos I 2005 *PRE'05: Proc. 1st Int. Workshop, Photoluminescence in Rare Earths: Photonic Materials and Devices (Trento, May 2005)* p 54
[23] Ovenstone J, Titler P J, Withnall R and Silver J 2001 *J. Phys. Chem.* B **105** 7170
[24] Wachtler M, Speghini A, Gatterer K, Fritzer H P, Ajò D and Bettinelli M 1998 *J. Am. Ceram. Soc.* **81** 2045
[25] http://www.webelements.com
[26] Falcomer D, Daldosso M, Speghini A, Bettinelli M, Enzo S, Lasio B and Musinu A 2006 submitted for publication
[27] Reisfeld R, Zigansky E and Gaft M 2004 *Mol. Phys.* **102** 1319
[28] Polizzi S, Fagherazzi G, Battagliarin M, Bettinelli M and Speghini A 2002 *J. Mater. Chem.* **12** 742
[29] Li J-G, Wang X, Watanabe K and Ishigaki T 2006 *J. Phys. Chem.* B **110** 1121
[30] Duffy N W, Peter L M, Rajapakse R M G and Wijayantha K G U 2000 *Electrochem. Commun.* **2** 262
[31] Duffy N W, Peter L M, Rajapakse R M G and Wijayantha K G U 2000 *J. Phys. Chem.* B **104** 8916
[32] Peter L M and Vanmackelberg D 1999 *Advances in Electrochemical Science and Engineering* ed R C Alkire and D M Kolb (Weinheim: Wiley)
[33] Dloczik L, Ileperuna O, Lauermann I, Peter L M, Ponomarev E A, Redmond G and Shaw N J 1997 *J. Phys. Chem.* B **101** 10281
[34] Nelson J, Haque S A, Klug D R and Durrant J R 2001 *Phys. Rev.* B **63** 205321
[35] Anta J A, Nelson J and Quirke N 2002 *Phys. Rev.* B **65** 125324
[36] Barzykin A V and Tachiya M 2002 *J. Phys. Chem.* B **106** 4356
[37] Cass M J, Qiu F L, Walker A B, Fisher A C and Peter L M 2003 *J. Phys. Chem.* B **107** 113
[38] Vanmaekelberg D and de Jough P E 2000 *Phys. Rev.* B **61** 4699
[39] Kambili A, Walzer A B, Qiu F L, Fisher A C, Savin A D and Peter L M 2002 *Physica* E **14** 203
[40] Schlichthorl G, Park N G and Frank A J 1999 *J. Phys. Chem.* B **103** 782
[41] Cao F, Oskam G, Mejer G J and Searson P C 1996 *J. Phys. Chem.* B **100** 17021
Ulherndorf I 1997 *J. Phys. Chem.* B **101** 10281
[42] Franco G, Gerhing L, Peter L M, Ponomarev E A and Ulhendorf I 1999 *J. Phys. Chem.* B **103** 692
[43] Peter L M and Wijayantha K G U 2000 *Electrochem. Commun.* **2** 658
[44] Fisher A C, Peter L M, Ponomarev E A, Walker A B and Wijayantha K G U 2000 *J. Phys. Chem.* B **104** 949
[45] Park N G, Van de Lagemaat J and Frank A J 2000 *J. Phys. Chem.* B **104** 8989
[46] Van de Lagemaat J and Frank A J 2001 *J. Phys. Chem.* B **105** 11194
Van de Lagemaat J and Frank A J 2002 *Syst. Nanostr.* **14** 203
[47] Enright B and Fitzmaurice D 1997 *J. Phys. Chem.* B **100** 1027
[48] Solbrand A, Henningsson A, Sodergre S, Lindstrom H, Hagfeldt A and Lindquist S A 1997 *J. Phys. Chem.* B **101** 2514
[49] Nakade S, Kambe S, Kitamura T, Wada Y and Yanagida S J 2001 *J. Phys. Chem.* B **105** 9150
[50] Beermann N 2002 *J. Photochem. Photobiol.* A **152** 213
[51] Forro L, Chauvet O, Emin D, Zuppiroli L, Berger H and Levy F 1994 *J. Appl. Phys.* **75** 633
[52] Mardare D 2005 *J. Opt. Adv. Mater.* **7** 721
[53] Park M S, Kwon S K and Min B I 2002 *Phys. Rev.* B **65** 161201(R)
[54] Jacoboni C and Reggiani L 1983 *Rev. Mod. Phys.* **55** 645
[55] Braglia G L 1977 *Physica* C **92** 91
[56] Rees H D 1968 *Phys. Lett.* A **26** 416
[57] Pines D 1963 *Elementary Excitations in Solids* (New York: Benjamin) p 273
[58] Engelsberg S and Schreiffer J R 1963 *Phys. Rev.* **131** 993
[59] Conwell E and Weisskopf V F 1950 *Phys. Rev.* **77** 388